Western North Pacific Tropical Cyclone Characteristics Stratified by Genesis Environment

HIRONORI FUDEYASU

Yokohama National University, Yokohama, Japan

RYUJI YOSHIDA

RIKEN Advanced Institute for Computational Science, and Research Center for Urban Safety and Security, Kobe University, Kobe, Japan

(Manuscript received 25 April 2017, in final form 27 November 2017)

ABSTRACT

The characteristics of tropical cyclones (TCs) in the summer and autumn seasons over the western North Pacific that are associated with different environmental factors that influence TC genesis (TCG) were studied. The authors objectively categorized factors into the five TCG factors classified by Ritchie and Holland: monsoon shear line (SL), monsoon confluence region (CR), monsoon gyre (GY), easterly wave (EW), and the Rossby wave energy dispersion from a preexisting TC (PTC). The GY-TCs tended to develop slowly, and the highest rates of occurrence of rapid intensification (RI) were found for the CR-TCs, whereas the GY-TCs rarely experienced RI. The average storm size of the GY-TCs at the time of formation was the largest of the averages among the TC types, while the EW- and PTC-TCs were smaller, although these differences disappeared at the mature time. There were no significant differences in the sea surface temperature (SST) beneath the TCs, but the tropical cyclone heat potential (TCHP) of the PTC-TCs was higher. The PTC-TCs tended to develop as intense TCs and exhibited favorable environmental characteristics, such as high TCHP, high convective available potential energy, and weak vertical shear. The occurrence rate of the PTC-TCs that made landfall in the Philippines was higher than the averages of the other TC types, whereas those of the EW-TCs (PTC-TCs) that made landfall in Japan (China) were lower. These results provide important information for use in disaster prevention.

1. Introduction

A tropical cyclone (TC) forms under large-scale environmental conditions favorable for cyclogenesis (TCG), which are generally found where sea surface temperatures (SSTs) exceed 26°C and supportive large-scale flow patterns coexist (Gray 1968, 1998). A large body of research on the large-scale environmental conditions favorable for TCG has been conducted (e.g., Emanuel and Nolan 2004; Camargo et al. 2007; McGauley and Nolan 2011; Korty et al. 2012).

Ritchie and Holland (1999, hereafter RH99) statistically investigated the environments of 199 TCG cases that occurred from 1984 to 1992 (excluding 1989) over the western North Pacific (WNP). They classified large-scale flow patterns in TCG into five factors: monsoon shear line (SL), monsoon confluence region (CR), monsoon gyre (GY), easterly wave (EW), and the Rossby wave energy dispersion from a preexisting TC (PTC). The SL is enhanced by the horizontal cyclonic shear associated with the monsoon trough over the WNP. The CR is mainly the zonal confluence zone between easterly trade winds and westerly monsoon winds at the eastern extremity of the monsoon trough. The GY has been recognized as a synoptic-scale gyre embedded within a developed monsoon trough (Lander 1994; Chen et al. 1996). These three factors (SL, CR, and GY) are closely related to Asian monsoons over the WNP. Gray (1968, 1998) reported that a monsoon trough is the most favorable environment for TCG.

The EW is related to the synoptic-scale trade easterly wind system. The trough of easterly trade winds provides an environment favorable for TCG (Heta 1990, 1991). The PTC is associated with a preexisting TC. A mature TC disperses its energy as a Rossby wave in a southeastward direction, and one of the low pressure areas of the wave train sometimes develops into a TC (McDonald 1998; Li and Fu 2006; Li et al. 2006). RH99 reported that the rate of occurrence of TCs controlled by the five TCG factors were as follows: SL accounts for

Corresponding author: H. Fudeyasu, fude@ynu.ac.jp

DOI: 10.1175/MWR-D-17-0110.1

42%, CR for 29%, GY for 3%, EW for 18%, and PTC for 8%.

Yoshida and Ishikawa (2013; hereafter YI13), building on the results of RH99, developed a method of detecting the environmental factors that contribute to TCG. The TCG detection method could objectively categorize TCG environments for each TC as one of the five factors defined by RH99. YI13 further extended the analysis period of TCG cases to 30 years, from 1979 to 2008. The results of their detection were similar to those of RH99.

Differences in the environmental factors that contribute to TCG could be considered as key determinants of the characteristics of TCs. For example, the tracks of TCs are greatly influenced by large-scale atmospheric circulations in the lower–midtroposphere over the TC life cycle, consisting of the Asian monsoon, midlatitude westerly winds, and easterly trade winds. It is, thus, possible that environmental factors influence not only TCG, but also the direction of movement of TCs, affecting the destination of the TC track. However, YI13 did not investigate the characteristics of TCs or the differences in environmental conditions stratified by the TCG environment.

This study revisited the dataset presented in YI13, extended through 2013, and statistically investigated the characteristics of TCs associated then with the environmental factors that influence TCG using information from best track data. The differences in the environmental physical parameters of the factors that influence TCG and affect the characteristics of TCs were also examined. The purpose of this study was to investigate how the different environmental factors contributing to TCG are related to the characteristics of the resulting TC.

The remainder of this paper is organized as follows. Section 2 introduces the methods of analysis. The statistical results are described in section 3. The influence of environmental factors that contribute to TCG on the characteristics of the resulting TCs are further discussed in section 4. The major results are summarized in the final section.

2. Methodology

a. TCG detection method

To separate TCG cases into categories influenced by the different environmental factors defined by RH99, the TCG detection method developed in YI13 was used in this study. Using reanalysis data, YI13 defined the SL, CR, GY, EW, and PTC with "contribution scores" for the flow patterns as an objective algorithm. This paper briefly reviews contribution scores $\mathrm{SCR_{SL}}$, $\mathrm{SCR_{CR}}$, $\mathrm{SCR_{GY}}$, $\mathrm{SCR_{EW}}$, and $\mathrm{SCR_{PTC}}$.

In YI13, the SL is identified as the location where the sign of the 850-hPa zonal wind component changes from negative on the northern side of the grid to positive on the southern side. The score for SL is calculated as follows:

$$\mathrm{SCR_{SL}} = A\left(\frac{\partial u}{\partial y}\right)_{\mathrm{ave}} \exp(B \times \mathrm{dist}), \tag{1}$$

where u is the zonal wind at the 850-hPa level, "dist" means the distance between the center grid of SL and the location of TCG, and A and B are arbitrary constants, with $A = -1.0$ and $B = -1.0 \times 10^{-5}$ for $\mathrm{SCR_{SL}}$. The location of each TCG was taken from the first record of the Joint Typhoon Warning Center (JTWC) best track data (Chu et al. 2002). An upper limit of 1500 km is set for the distance, and the SL score is not calculated when "dist" exceeds the upper limit.

The contribution scores for the CR and EW patterns are defined as the border between westerly and easterly zonal winds and as the intensity of the west–east shear of the meridional winds near the trough, respectively. These scores are calculated using the equations below:

$$\mathrm{SCR_{CR}} = A\left(\frac{\partial u}{\partial x}\right)_{\mathrm{ave}} \exp(B \times \mathrm{dist}), \tag{2}$$

$$\mathrm{SCR_{EW}} = A\left(\frac{\partial v}{\partial x}\right)_{\mathrm{ave}} \exp(B \times \mathrm{dist}), \tag{3}$$

where v is the meridional wind at the 850-hPa level, and A and B are arbitrary constants, with $A = -1.0$ and $B = -1.0 \times 10^{-5}$ for $\mathrm{SCR_{CR}}$ and $A = 2.0 \times 10^{-1}$ and $B = -1.0 \times 10^{-2}$ for $\mathrm{SCR_{EW}}$. An upper limit of 1500 km is set for the distance for $\mathrm{SCR_{CR}}$.

The GY pattern is evaluated using the similarity of the 850-hPa wind field to a composite of typical GY cases reported by Lander (1994), with the score for GY and the degree of pattern matching M determined as follows:

$$\mathrm{SCR_{GY}} = \exp(-M) \times (\zeta - \zeta_{\mathrm{std}}), \tag{4}$$

$$M = \sum_{i=0}^{ni} \sum_{j=0}^{nj} \sqrt{(C'_{(i,j)} - \mathrm{data}'_{(i,j)})^2}, \tag{5}$$

where ζ is the relative vorticity, which is expressed as the excess above the standard value $\zeta_{\mathrm{std}} = -1.0 \times 10^{-5}$. For M [Eq. (5)], C' is the model GY pattern sea level pressure (SLP) field, data′ is the corresponding SLP field of a given TCG case, i and j represent the horizontal grid, and ni and nj are the width and length, respectively.

Based on the previous discussion (Li and Fu 2006; Li et al. 2006), the contribution of PTC is estimated according to the amplitude of the wave closest to the PTC after searching for a preexisting TC northwest of the

TCG location. Once a preexisting TC is found, we compute the amplitude of the first Fourier component C^2_{wv1} of SLP along the line connecting the preexisting TC and TCG locations with the score for PTC, as follows:

$$SCR_{PTC} = C^2_{wv1}. \quad (6)$$

A lower limit of 1.01, derived by the empirical method, is set for C^2_{wv1}.

Each score (SCR_x) is finally normalized by its maximum value [$Max(SCR_x)$] and minimum value [$Min(SCR_x)$] derived in the latest 30 years, as follows:

$$SCR_x = \frac{SCR_x - Min(SCR_x)}{Max(SCR_x) - Min(SCR_x)}. \quad (7)$$

Along with the final scores after normalization, the maximum contribution score is determined as the major flow pattern contributing to the TCG, namely, the SL, CR, GY, EW, and PTC. When the major TCG factor could not be determined by the TCG detection method, it was considered to be unclassified flow (UCF). See YI13 for the specific details of the TCG detection method.

For the TCG detection method, this study used 850-hPa wind and SLP derived from the Japanese 25-year Reanalysis Project (JRA-25; Onogi et al. 2007) (http://jra.kishou.go.jp/JRA-25/index_en.html). The JRA-25 was collected every 6 h between 1979 and 2013, with a horizontal resolution of 1.25° for both longitude and latitude. The analysis period of this study was 35 years, from 1979 to 2013, which is the same as the available period of JRA-25. We extended the analysis period of the TCG cases used in YI13, which investigated the period of 1979 to 2008.

b. Data and environmental physical parameters

Although YI13 analyzed the TCG factors from all TCs, including tropical depressions (TDs), this study focused only on TCs of tropical storm (TS) or greater intensity, that is, maximum 1-min sustained wind speed in excess of 17.2 m s^{-1} or 34 kt. This study analyzed the characteristics of TCs associated with each factor that influences TCG using TC data derived from the International Best Track Archive for Climate Stewardship (IBTrACS; Knapp et al. 2010) at the time of TS formation (TSF) and mature time. The time of TSF was defined as the time when minimum TS intensity was reached, and the mature time was defined as the time when the maximum wind speed occurred. It should be noted that the time of TSF was usually different from the time of TCG, which is the first record in the JTWC best track data in YI13. This study focused on the time of TSF and the mature time for two reasons: the characteristics and conditions of TCs at both of these times are important for disaster prevention and mitigation, and both times were suitable for comparing the characteristics of a TC among the different TCG factors.

For each factor that influences TCG, the relationship between the average influence due to each factor and the other factors was assessed at the 5% significance level using a t test that indicates significant differences versus all systems. For example, the average of the SL was compared to the average influence of the other factors, that is, the CR, GY, EW, PTC, and UCF.

This study also investigated the differences in the environmental physical parameters among factors that influence TCG: the magnitude of the vertical shear, lower- and midtropospheric humidity, maximum potential intensity (MPI; Emanuel 1986), convective available potential energy (CAPE) derived from the MPI equation, SST, tropical cyclone heat potential (TCHP), depth of the 26°C isotherm in the ocean, and sea surface 100-m depth-averaged ocean temperature. The magnitude of the vertical shear was defined as the difference in horizontal winds between the 850- and 200-hPa levels, which were the averages of a 5° × 5° box relative to the center of the TC, using the JRA-25. The lower- and midtropospheric humidities were defined as the mixing ratio at the 850- and 500-hPa levels, respectively, which were averages of a 5° × 5° box relative to the TC center, using the JRA-25.

The information on the ocean was derived from the three-dimensional variational-based parent domain output from the Four-dimensional Variational Ocean Reanalysis for the Western North Pacific (FORA-WNP30; Usui et al. 2017; http://synthesis.jamstec.go.jp/FORA/). The data have a horizontal resolution of 0.5° for both longitude and latitude, with 54 vertical levels from 0.5- to 6000-m depth and a 6-h time interval from 1982 to present. Using FORA-WNP30, the TCHP was calculated by summing the ocean heat content from the surface down to the depth of the 26°C isotherm (Leipper and Volgenau 1972; Wada 2015) as follows:

$$Q = C_p \sum_{z=0}^{Z26} \rho_i (T_i - 26) \Delta z_i, \quad (8)$$

where Q is the TCHP value (J cm^{-2}), C_p is specific heat at constant pressure, T_i is water temperature (°C), Δz is water layer thickness, and ρ is the density of water. The parameter Z26 is the depth (m) of the 26°C isotherm.

Using the JRA-25 and FORA-WNP30, this study examined the differences in the MPI and CAPE. The MPI was proposed originally by Emanuel (1986), and the MPI and CAPE revised by Bister and Emanuel (1998) were used to account for dissipative heating. The MPI and CAPE were calculated as averages of a 5° × 5°

box relative to the TC center. Note that the SST was used at the TC center to create distinct features stratified by TCG environment.

The equivalent blackbody temperatures T_{BB}, derived from the merged IR channels from five geostationary satellites of the Climate Prediction Center (http://www.cpc.ncep.noaa.gov/products/global_precip/html/wpage.merged_IR.shtml), were used to describe the cloud features of TCs for each TCG factor. These data were defined on a 4-km horizontal grid for every 1-h period.

3. Results

a. Genesis number and seasonal changes

The total number and percentage of TCs that reached TS or greater intensity influenced by each environmental factor over the analysis period from 1979 to 2013 were as follows: among the 874 TCs, the most frequent influencing factor was SL (396 TCs, 46% of the total), followed by CR (157 TCs, 18%) and EW (119 TCs, 14%). PTC (83 TCs) and GY (78 TCs) accounted for 9% each, and UCF (41 TCs) accounted for 4%.

The seasonal changes in the formation of TCs influenced by the five environmental factors and UCF were also examined. The SL- and EW-TCs (hereafter, SL-TC, EW-TC, and similar terms indicate a TC that formed in a large-scale flow mainly associated with an SL, EW, or similar factor) occurred throughout the year, whereas the CR-, GY-, and PTC-TCs rarely occurred in winter and spring. The number of the CR- and GY-TCs, which are related to Asian monsoon activity, tended to increase in the summer, while the PTC-TCs tended only to occur in the summer and autumn, when many TCs were formed. Seasonal changes in the number of the SL- and EW-TCs, therefore, were less significant than changes in the numbers of the CR-, GY-, and PTC-TCs. The seasonality of the TCs of TS or greater intensity was similar to that reported by YI13, who considered environmental factors for all TCs, including TDs.

b. Tropical storm formation location

As shown in the previous section, seasonality in TCG is different for TCs influenced by different environmental factors. To compare the characteristics of a TC among the different TCG factors correctly, this study considered 677 TCG cases in the summer and autumn seasons from June to November (Table 1), when any of the influencing factors could occur frequently. Even when the analysis period was limited in this way, the proportional occurrence of the factors that influenced TCG was almost the same as the result obtained over the whole period.

Table 1 shows the average location of TSF for each factor that influenced TCG over the 35-yr analysis period between June and November. There were significant differences in the average location of TSF for the SL, EW, and PTC. EW- and PTC-TCs occurred, on average, farther to the east than other types of TCs, and this difference was significant at the 5% level. In contrast, the location of TSF of the SL-TCs was more biased to the west than that of other types of TCs. Additionally, the EW-TCs (PTC-TCs) occurred, on average, farther to the north (south) than other types of TCs.

If this study examines the distribution of the location of TSF in detail, it is clear that the situation for each environmental factor was different. Figure 1 shows the location of TSF classified into the factors that influenced TCG over the 35-yr analysis period between June and November. The location of TSF of the SL-TCs extended from the west to the east, where the SL was formed by the westerly monsoon and eastward winds. Many locations of TSF of the CR-TCs were located over the eastern Philippine Sea, where a confluence area is likely formed. The EW-TCs were generally located in the eastern part of the WNP, most likely due to the easterly winds coming from the eastern North Pacific. Because the PTC-TCs form on the southeastern side of a preceding TC, it is rare for them to form in the northern part of the WNP and the South China Sea, resulting in significant differences in the average location between the PTC-TCs and the other types of TCs.

c. Intensity

There were no differences in the average intensity of TCs generated by different environmental factors at the time of TSF because this was the time when all TCs reached TS intensity. However, the rate of development, defined by the increase in the maximum wind speed 1 day after the time of TSF, was significantly different. The rate of development of the GY-TC was slower than the rate of the other types of TCs, with the difference being significant at the 5% level (Table 1).

Rapid intensification (RI) for a TC is defined here as an increase in wind speed of 17.2 m s^{-1} or more in 24 h. Over the 35-yr analysis period between June and November, 96 TCs (14% of the total) experienced RI. Among the TCs generated by different environmental factors, the occurrence of RI for the SL-TCs was the largest (43 TCs), followed by the CR-TCs (25 TCs) and the EW- and PTC-TCs (10 TCs). Only six GY-TCs experienced RI. To compare environments favorable for RI correctly, rates of RI occurrence were divided by the number of occurrences of each environmental factor that influence TCG, as shown in Fig. 2. The rate of occurrence of RI for the SL (14%) was the same as the

TABLE 1. Statistical summary of the parameters associated with the environmental factors that influenced TCG over the 35-yr analysis period between June and November. Areas where a *t* test indicates significant differences with a 5% level of significance are presented in boldface font.

		SL	CR	GY	EW	PTC	UCF	ALL
Time of TSF	No.	300 (44%)	130 (19%)	61 (9%)	92 (14%)	66 (10%)	28 (4%)	677
	Avg lat (°N)	16.8	17.4	16.4	**17.9**	**13.9**	**19.8**	**16.9**
	Avg lon (°E)	**134.2**	133.5	133.4	**138.3**	**140.8**	132.2	135.1
	Radius of 30-kt wind (n mi, 1 n mi = 1.852 km)	115.2	111.6	**129.5**	**104.7**	**102.3**	**125.5**	113.6
	RMW (km)	38.4	37.9	**43.1**	36.7	39.2	39.1	38.1
One day after time of TSF	Δlon (°)	−2.2	**−1.9**	−2.0	**−2.7**	**−3.4**	−1.6	−2.3
	Δlat (°)	1.8	**2.0**	1.7	1.7	**1.3**	1.8	1.8
	Δwind (kt)	13.4	13.0	**11.4**	15.0	13.7	**9.8**	13.3
Mature time	Duration from TSF (day)	3.2	3.0	3.0	2.9	**3.9**	3.0	3.2
	Max wind (kt)	69.7	67.5	68.9	69.9	**77.0**	**63.0**	69.7
	Min pressure (hPa)	959.6	963.3	961.5	960.5	**953.1**	968.1	960.3
	Radius of 30-kt wind (n mi)	226.5	220.5	246.4	241.0	**255.0**	220.4	231.7
	RMW (km)	24.0	26.9	22.3	24.9	**18.5**	26.7	24.5
Decaying time	Duration from TSF (day)	5.3	5.2	5.3	5.3	**6.5**	4.7	5.4

average (the climatology of all TCs; 14%). The rate of occurrence of RI for the GY-TCs (9%) was smaller than the rate of occurrence of RI among all TCs, meaning that the GY-TCs experienced RI more rarely than the other types of TCs. The low rate of RI for the GY-TCs is related to their slower development versus the other types of TCs at the time of TSF. It is interesting to note that the rate of occurrence of RI was the highest for the CR-TCs (19%), that is, more than 2 times that of the GY-TCs.

At the mature time, there was a significant difference in the average intensity (Table 1): the PTC-TCs tended to have lower central pressure and higher maximum winds. To determine the tendency of an intense TC to develop, this study also examined the occurrence of specific classes of TC intensity categorized using the Saffir–Simpson hurricane wind scale (Simpson 1974). Over the 35-yr analysis period between June and November, one category 5 (more than 70 m s^{-1} or 135 kt) TC, 14 category 4 (59–69 m s^{-1} or 114–134 kt) TCs, and 86 category 3 (50–58 m s^{-1} or 96–113 kt) TCs were classified as major TCs, that is, having a maximum wind speed of 50 m s^{-1} (96 kt) or more. Among the major TCs, the SL-TCs were the most frequent (44), followed by the CR-TCs (18), the EW-TCs (14), and the PTC-TCs (11). The rate of occurrence divided by the number of occurrences for each environmental factor that influenced TCG is shown in Fig. 3. The rate of occurrence of major TCs for the SL-TCs (15%) was the same as the average (15%). Interestingly, the rate of occurrence

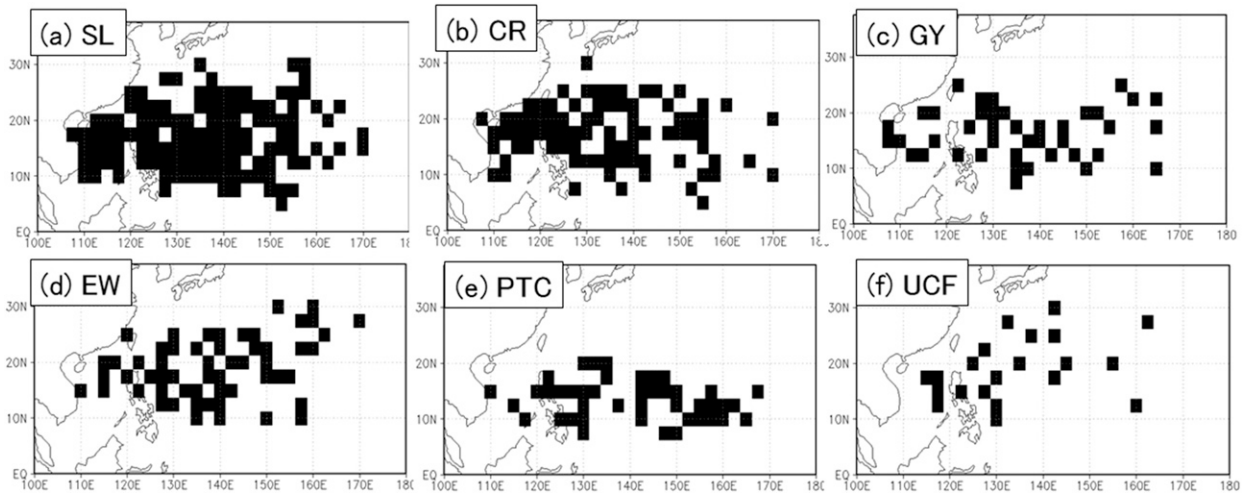

FIG. 1. The locations of TS formation of (a) SL, (b) CR, (c) GY, (d) EW, (e) PTC, and (f) UCF over the 35-yr analysis period between June and November. Shading indicates areas of numbers greater than one.

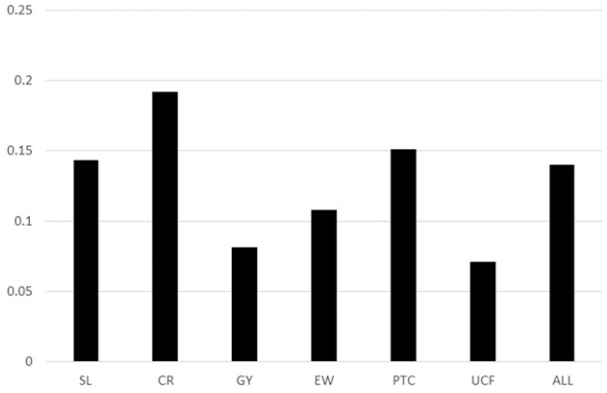

FIG. 2. Rate of occurrence of RI divided by the number of occurrences of each environmental factor that influences TCG over the 35-yr analysis period between June and November.

for the PTC-TCs was 22%, which was about 50% higher than the average. By contrast, among "weak TCs," that is, TSs, the rate of occurrence of the PTC-TCs was 24%, which was about half that of the climatology (42%). This means that the PTC-TCs tended to develop into intense TCs but rarely remained at the intensity of weak TCs.

d. Storm size

The storm size of TCs in the horizontal direction was defined as the radius of the 30-kt ($1\,\text{kt} = 0.5144\,\text{m s}^{-1}$) sustained wind provided by the Regional Specialized Meteorological Center (RSMC) Tokyo Typhoon Center of the IBTrACS. There was a significant difference at the time of TSF (Table 1). The average 30-kt wind radius of the GY-TCs was about 20% larger than that of the other types of TCs, whereas the EW- and PTC-TCs were smaller. In addition, this study examined the radius of maximum wind (RMW) provided by the JTWC of the IBTrACS. The RMW of the GY-TCs was large at the time of TSF, and this difference from the other types of TCs was significant at the 5% level.

Figure 4 shows composites of the T_{BB} distribution made with respect to TC centers during the period between the time of TSF and 12 h before the time of TSF. The region of low T_{BB} (<270 K) near the center corresponds to the cloud cluster of TC, and the size of the cloud cluster of the EW- and PTC-TCs is small. By contrast, the low T_{BB} of the GY-TCs has an asymmetric structure extending from the northeast to the southwest.

Interestingly, the storm size of TCs at the mature time did not differ significantly from the average TCG, except for the PTC-TCs (Table 1). In other words, the storm size of the EW- and GY-TCs did not affect the future storm size at the mature time, although there were significant differences at the time of TSF. The RMW of PTC-TCs was small at the mature time, whereas the radius of 30-kt sustained winds increased with the increases in the intensity of PTC-TCs.

e. Life span and track

Table 1 shows the averages of two measures of TC duration; one is the duration of the developmental stage, that is, from the time of TSF to mature time, and the other is the life span from the time of TSF to the decaying time. The decaying time was defined as the point at which the system had TS intensity for the final time. The duration of the developmental stage differed with a 5% level of significance. The mean duration of the PTC-TCs was 3.9 days, which was approximately 20% longer than the average of 3.2 days. The longer mean duration of the PTC-TCs was likely due in part to the farther-southeast TSF location. The longer duration of the developmental stage contributed to the life span of the PTC-TCs being longer than those of the other TCG types.

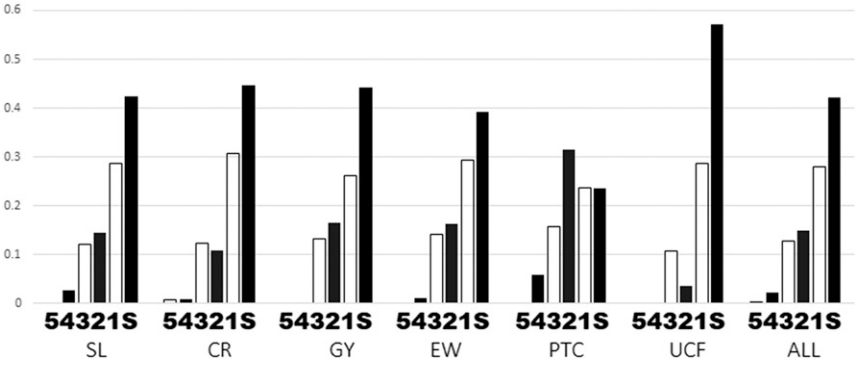

FIG. 3. Rates of occurrence of different classes of TC intensity divided by the number of occurrences of each environmental factor that influences TCG over the 35-yr analysis period between June and November. The classes are defined as maximum 1-min sustained wind speed; TS and the Saffir–Simpson hurricane wind scale. Note: category 5 is 5; category 4, 4; category 3, 3; category 2, 2; category 1, 1; and TS, S.

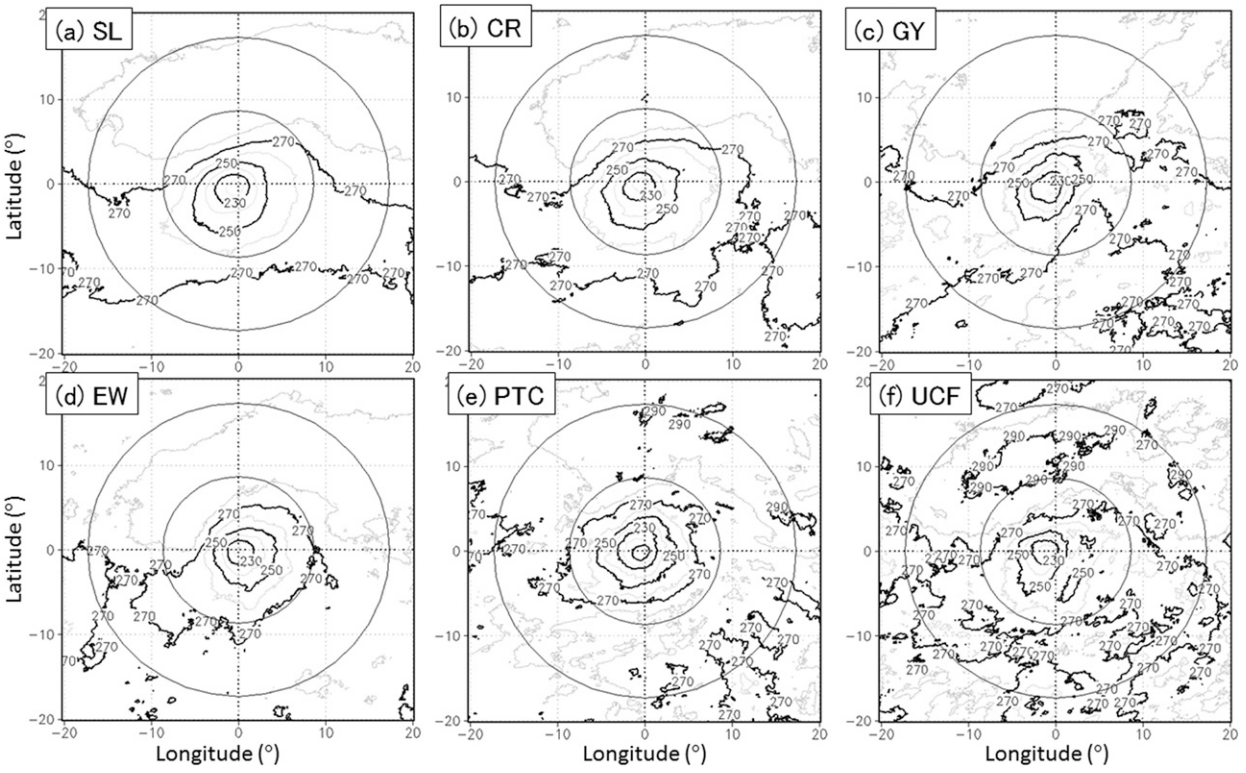

FIG. 4. Composites of T_{BB} distributions of (a) SL, (b) CR, (c) GY, (d) EW, (e) PTC, and (f) UCF over the 35-yr analysis period between June and November. The composite was made with respect to the centers of TCs from the time of TSF to 12 h before the time of TSF. The contour interval is 10 K. The bold contour indicates 230, 250, and 270 K.

The movements of TCs according to their TCG factors were investigated, and Fig. 5 shows the tracks of TCs. Also, the direction of movement at the time of TSF, as shown in Table 1, was defined as the distance moved by the east–west and the north–south components from the time of TSF to 1 day later. The EW- and PTC-TCs tended to move westward at the time of TSF, and this difference from the other types of TCs was significant at the 5% level. Additionally, the distance of northward movement of the PTC-TCs was less than that of other types of TCs. By contrast, the westward distance moved by the CR-TCs was less than that moved by other types of TCs; the CR-TCs tended to move northward. Because the CR-TCs mainly form at the eastern extremity of westerly monsoon winds, the CR-TCs rarely moved westward.

Along the destination of the track, the number of landfalls in each country (Japan, China, Vietnam, and the Philippines) was statistically investigated. This study adopted the definition of a TC landfall as the intersection of the TC track with a coastline, as described by Fudeyasu et al. (2014). Countries bordering the WNP experience the highest number of TC landfalls in the world (Fudeyasu et al. 2014). In all, 89 TCs (13%) made landfall in Japan in the 35-yr analysis period between June and November. Among these, the SL-TCs were the most frequent (47), followed by the CR-TCs (22). The rate of occurrence divided by the number of occurrences for each environmental factor that influenced TCG (Table 1) is shown in Fig. 6 and Table 2. The rate of occurrence for the CR-TCs (17%) was almost the same as that for the SL-TCs (16%). As the rate of occurrence for the EW-TCs (5%) was very low, the EW-TCs moved toward Japan more rarely than the other types of TCs. The low rate of occurrence of the EW-TCs that made landfall in Japan was likely influenced by the westward trend of TC movement at the time of TSF (Table 1).

The rates of occurrence of the TCs that made landfall in the other countries varied, as shown in Fig. 6 and Table 2. The rate of occurrence of TCs that made landfall in China was lowest for the PTC-TCs, among the other TC factors, while the rate in the Philippines was highest for PTC-TCs. The results obtained from this statistical analysis provide important information for disaster prevention.

f. Environmental physical parameters

Table 3 shows the averages of the atmospheric environmental physical parameters—the lower- and

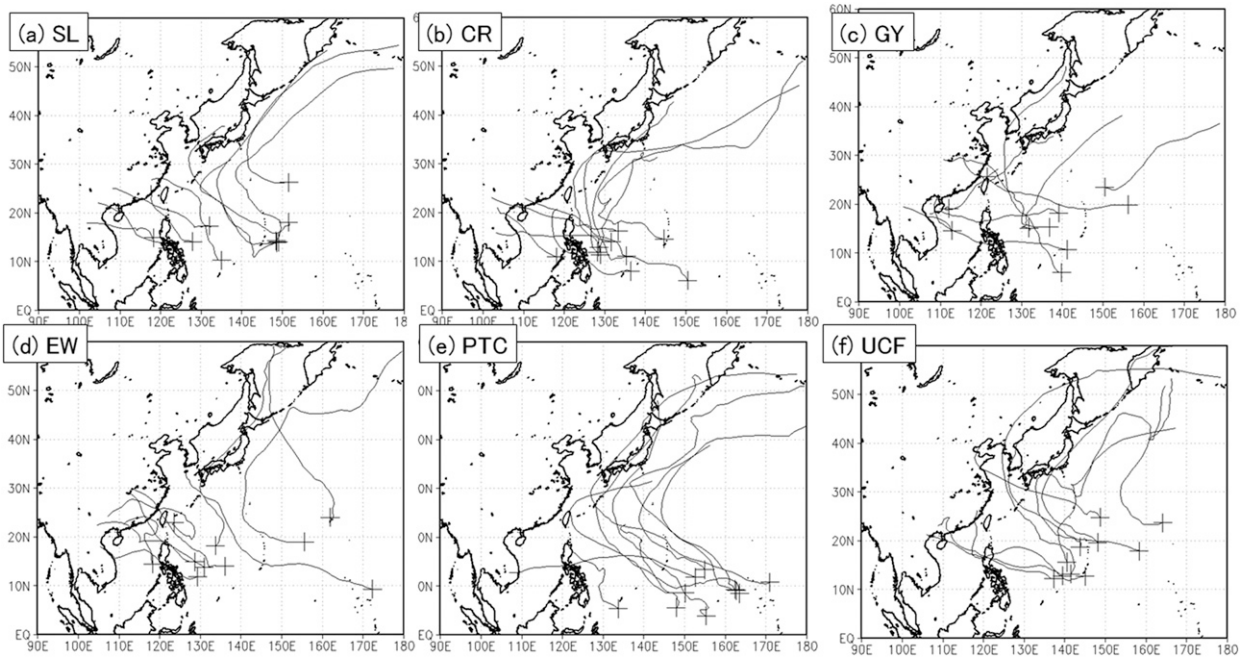

FIG. 5. TC tracks (lines) and first locations (crosses) of (a) SL, (b) CR, (c) GY, (d) EW, (e) PTC, and (f) UCF. The tracks represent 10 recent TSs for each environmental factor.

midtropospheric humidity, zonal and meridional vertical shear, magnitude of the vertical shear, CAPE, MPI maximum wind, and TC central pressure—averaged to within 5° of the TC center at both the time of TSF and mature time. Additionally, Table 4 shows the following ocean environmental physical parameters beneath the TC center: SST, TCHP, depth of the 26°C isotherm in the ocean, and sea surface 100-m depth-averaged ocean temperature. Statistical analyses for the atmospheric parameters were used to associate TCs with each factor over the 35-yr analysis period between June and November, while analysis periods for ocean parameters were from 1982 to 2013, the same as the available period of FORA-WNP30.

The lower- and midtropospheric humidity differed among factors, with a 5% level of significance (Table 3). Relatively wet conditions in the SL and CR environments were apparent at both TSF and mature times. By contrast, the lower- and midtropospheric humidity for EW were lower than those for the other types of TCs. The relatively drier conditions around the EW-TCs were apparent throughout the troposphere (not shown). The drier conditions were linked to the average storm size of the EW-TCs at the time of TSF, smaller than the other types of TCs (Table 1 and Fig. 4).

It is interesting that there were no significant differences in average SST at both the TSF and mature times, except for those of UCF (Table 4 and Fig. 7). However, at the time of TSF, the TCHP and sea surface 100-m depth-averaged temperature of the PTC were higher, and the depth of the 26°C isotherm was deeper, compared to the other types of TCs. This ocean condition of PTC was likely due in part to the TSF location being farther southeast.

At both the TSF and mature times, the maximum wind and central pressure of the MPI for the PTC-TCs were significantly intensified, most likely as a result of the higher CAPE (Table 3). With a longer duration of development under the weak vertical shear and higher TCHP, the large-scale environments associated with PTC were favorable for TC development.

Although relatively wet conditions in the CR environments were apparent at the mature time, the central pressure of the MPI for the CR was significantly higher. The exact reasons why the environments associated with the CR at the mature time were less favorable remain unclear.

4. Discussion

The storm sizes of the EW-, GY-, and PTC-TCs generated by different environmental factors differed significantly at the time of TSF. According to the results of an idealization experiment conducted by Xu and Wang (2010), whose experimental design followed Wang (2009), the simulated size of a TC defined as the radius of azimuthal mean damaging-force wind

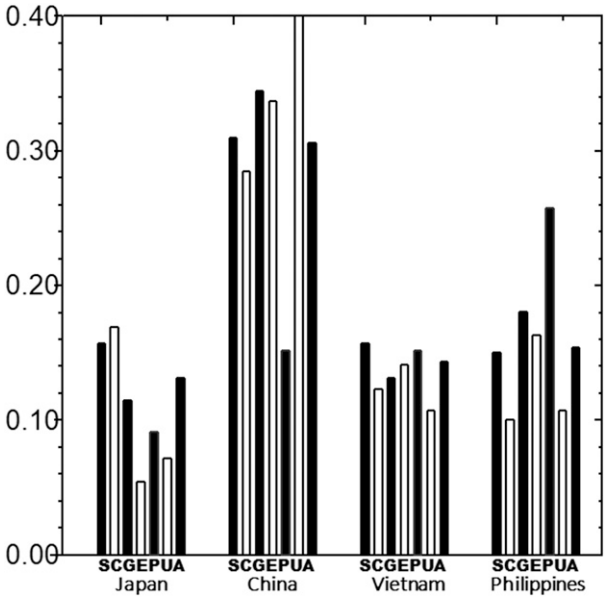

FIG. 6. The rate of occurrence of TCs that made landfall in Japan, China, Vietnam, and the Philippines, by country, divided by the number of occurrences of each environmental factor that influenced TCG over the 35-yr analysis period between June and November. Note: monsoon shear line is S; monsoon confluence region, C; monsoon gyre, G; easterly wave, E; Rossby wave energy dispersion, P; unclassified flow, U; and average of all TCs (i.e., climatology), A.

($25.7\,m\,s^{-1}$) was largely determined by the horizontal size of the large-scale initial circulation field. In their study, strong winds in an initial large-scale circulation led to the development of active spiral rainbands. The latent heat released in spiral rainbands played a key role in increasing the low-level radial inflow and accelerating tangential winds outside, resulting in the outward expansion of tangential wind fields and, thus, increasing the size of the TC.

It was found that the storm size of a GY-TC at the time of TSF was larger than other types of TCs, but the EW- and PTC-TCs were smaller. In the large-scale environment associated with the GY, a TC could form within the monsoon trough, where the initial large-scale circulation field was large. By contrast, the EW-TCs were associated with a trough of easterly trade winds, and the PTC-TCs formed in the low pressure areas of the wave train as the Rossby wave energy dispersed from a preexisting TC, where large-scale circulation was relatively small. This is consistent with the results of Xu and Wang (2010).

While the TCG detection method used for classification accounted for most of the TCG mechanisms, there were 41 TCs with an unclassified flow. The features of UCF-TCs were a more northerly location of TSF and a larger average size and slower development at the time of TSF, as well as weaker intensity at the mature time, compared with the other types of TCs. Given the features of the UCF-TCs, it is worth considering whether there could be another genesis mechanism. Davis and Bosart (2003, 2004, 2006) found the mechanism of tropical transition: the system begins as an extratropical cyclone, which occludes and drifts within subtropical latitudes; convection builds, and then there is full transition to a TC structure. However, this study did not find any significant effect from an extratropical cyclone on the TCG of UCF-TCs in weather charts. The mechanism of tropical transition has been linked primarily to TCG in the Atlantic basin but not TCG in the WNP. Because the purpose of this study was to investigate the characteristics of TCs stratified by TCG environment, the clarification of unclassified flow modifying the TCG detection method is reserved for future studies.

5. Conclusions

This study used the TCG detection method to categorize intense TCs according to the environmental factors that influenced TCG over the WNP for a 35-yr period. Examining seasonal changes in TCG cases for each environmental factor that influenced TCG led to the conclusion that the SL- and EW-TCs occurred annually, whereas CR-, GY-, and PTC-TCs mainly occurred in the summer and autumn. The characteristics of TCs associated with the different factors were studied using 677 TCG cases that occurred between June and November, when all of the environmental factors could occur. Our results can be summarized, as synthesized schematically in Fig. 8, as follows:

TABLE 2. Statistical summary of the number and rate of occurrence of TCs making landfall in Japan, China, Vietnam, and the Philippines, divided by the number of occurrences of each environmental factor that influenced TCG over the 35-yr analysis period between June and November.

	SL	CR	GY	EW	PTC	UCF	ALL
Japan	47 (16%)	22 (17%)	7 (11%)	5 (5%)	6 (9%)	2 (7%)	89 (13%)
China	93 (31%)	37 (28%)	21 (34%)	31 (34%)	10 (15%)	15 (54%)	207 (31%)
Vietnam	47 (16%)	16 (12%)	8 (13%)	13 (14%)	10 (15%)	3 (11%)	97 (15%)
Philippines	45 (15%)	13 (10%)	11 (18%)	15 (16%)	17 (26%)	3 (11%)	104 (14%)

TABLE 3. As in Table 1, but for the atmospheric environmental physical parameters averaged to within 5° of the TC center over the 35-yr analysis period between June and November. Areas where a *t* test indicates significant differences with a 5% level of significance are presented in boldface font.

		SL	CR	GY	EW	PTC	UCF	ALL
Time of TSF	850-hPa mixing ratio (kg kg^{-1})	**0.928 31**	0.927 91	0.928 58	**0.926 11**	0.927 72	0.927 87	0.927 89
	500-hPa mixing ratio (kg kg^{-1})	**0.769 92**	**0.771 47**	0.772 01	0.746 05	**0.764 05**	0.767 98	0.766 510
	Zonal vertical shear (m s^{-1})	−1.5	−1.9	−1.8	**0.2**	−2.1	−2.4	−1.4
	Meridional vertical shear (m s^{-1})	−1.9	**−2.7**	−1.8	**−1.0**	−1.5	−1.8	−1.9
	Total vertical shear (m s^{-1})	6.2	**6.6**	6.5	5.8	**5.5**	5.8	6.1
	CAPE (J kg^{-1})	13 074.4	12 978.8	12 837.9	13 247.1	**13 651.5**	**12 096**	13 073.9
	MPI maximum wind (m s^{-1})	115.7	115.8	114.7	116.5	**118.4**	**110.9**	115.7
	MPI central pressure (hPa)	858.1	859.2	860.4	858.0	**853.8**	**868.5**	858.5
Mature time	850-hPa mixing ratio	**0.928 75**	**0.929 04**	0.928 61	**0.925 60**	0.927 56	0.927 71	0.928 21
	500-hPa mixing ratio	0.773 53	**0.776 41**	0.776 73	**0.756 19**	**0.760 14**	0.785 71	0.771 11
	Zonal vertical shear	−0.7	−1.0	−0.8	0.4	−0.0	−0.2	−0.5
	Meridional vertical shear	−0.7	**−2.0**	−0.2	0.0	**0.4**	−1.0	−0.7
	Total vertical shear	**8.0**	7.6	7.5	7.7	**6.6**	**6.2**	7.6
	CAPE	10 331.2	10 007.0	10 031.2	10 526.9	10 468.0	**9402.3**	10 249.8
	MPI maximum wind	99.6	**94.4**	98.5	100.1	**102.7**	**87.8**	98.4
	MPI central pressure	881.7	**889.8**	884.7	881.5	**878.0**	**898.8**	883.8

- The average location of TSF of the EW-TCs (PTC-TCs) was farther east and north (south), while that of the SL-TCs was farther west than those of the other types of TCs.
- The average size of the GY-TCs at the time of TSF was larger than that of the other types of TCs, while the EW- and PTC-TCs were smaller.
- The average size of the RMW of the GY-TCs at the time of TSF was larger than the average of the other types of TCs, while the RMW of the PTC-TCs at the mature time was smaller.
- The GY-TCs tended to develop slowly at the time of TSF.
- Rates of RI occurrence for the CR-TCs were higher than for the other types of TCs, whereas the GY-TCs rarely experienced RI.
- The EW- and PTC-TCs tended to move westward at the time of TSF. Conversely, the CR-TCs tended to move northward.
- The occurrence rate of the PTC-TCs that made landfall in the Philippines was higher, and those of the EW-TCs (PTC-TCs) that made landfall in Japan (China) were lower, than the average for all TCs.
- The duration of the developmental stage and the TC life span of the PTC-TCs were longer than for the other types of TCs.
- There were no significant differences in the average storm size of TCs at the mature time, except for the PTC-TCs, which were larger than the other types of TCs.
- The PTC-TCs tended to develop as intense TCs in the environments favorable for TC development.
- According to MPI theory, the large-scale environments associated with the PTCs were more favorable for TC development.
- There were no significant differences in SST around the TCs at the both of TSF and mature times, except for UCF-TCs.

TABLE 4. As in Table 1, but for the ocean environmental physical parameters beneath the TC center over the 32-yr analysis period between June and November. Areas where a *t* test indicates significant differences with a 5% level of significance are presented in boldface font.

		SL	CR	GY	EW	PTC	UCF	ALL
Time of TSF	SST (°C)	29.0	29.0	28.9	29.0	29.0	**28.7**	29.0
	TCHP (kJ cm^{-2})	81.1	78.5	76.2	80.9	92.9	66.2	80.7
	Depth of the 26°C isotherm (m)	80.1	77.4	76.9	78.6	**90.3**	**67.6**	79.6
	0–100-m average temperature (°C)	27.1	27.1	27.0	27.0	**27.9**	**26.5**	27.1
Mature time	SST	27.8	27.9	27.9	27.8	27.8	27.6	27.8
	TCHP	40.2	40.5	**34.6**	40.3	41.0	42.0	40.3
	Depth of the 26°C isotherm	51.2	49.6	**44.5**	50.7	55.5	48.6	50.8
	0–100-m average temperature	25.0	24.9	24.7	24.9	25.3	24.3	24.9

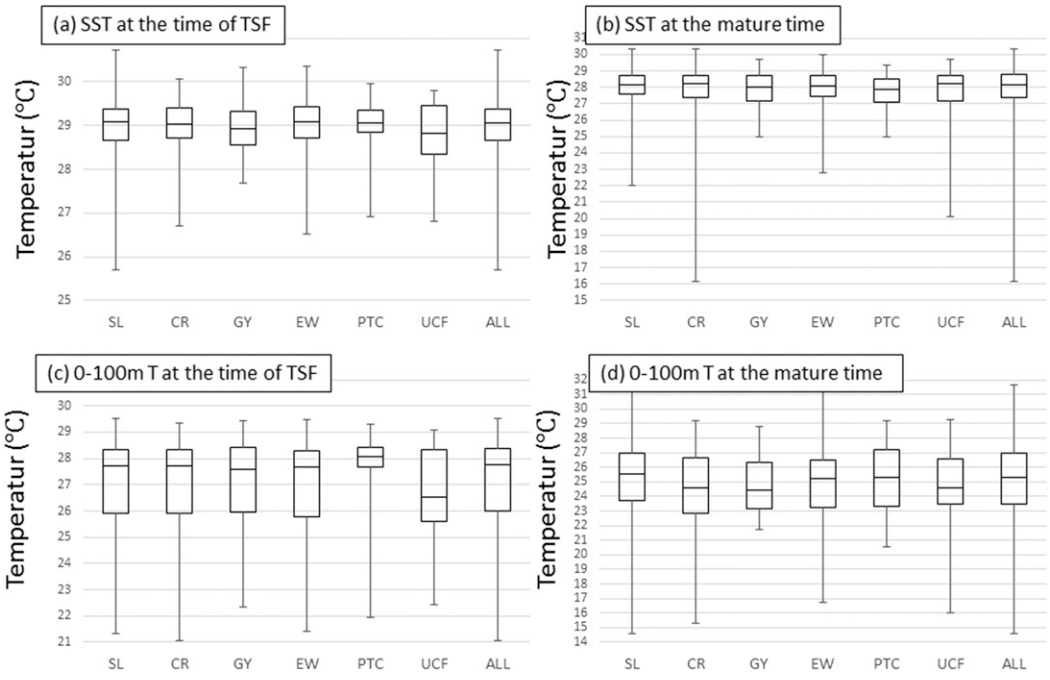

FIG. 7. Boxplots of (a),(b) SST and (c),(d) sea surface–100-m depth-averaged ocean temperature of each environmental factor that influenced TCG at (a),(c) the time of TSF and (b),(d) the mature time over the 32-yr analysis period between June and November. The vertical bar shows the full range of the distributions, and the box shows the interquartile range of 25%–75% of all cases. The bold horizontal line within each box indicates the median.

- The TCHP and the sea surface100-m depth-averaged temperature of the PTC-TCs at the time of TSF were higher, with deepening of the depth of the 26°C isotherm.
- The lower- and midtropospheric humidity values were higher for the SL- and CR-TCs, but lower for the EW-TCs, than for the other types of TCs.

The exact reasons why CR-TCs tended to experience RI remain unclear. Furthermore, the UCF-TCs that were not categorized by this TCG detection method are not yet well understood. However, the relationship between large-scale environmental factors that influence TCG and the characteristics of TCs can be used in cyclogenesis studies from a climate perspective, and the trends for landfall in each country will be important for disaster prevention.

Acknowledgments. The authors thank Drs. K. Ito, A. Wada, M. Yamaguchi, C. Muroi, K. Bessho, and N. Koide for their helpful comments and support of data analysis. The authors are also grateful for the assistance of laboratory members from the Yokohama National University. This study utilized the dataset of JRA-25, the cooperative research project carried out by the Japan Meteorological Agency (JMA) and the Central Research Institute of Electric Power Industry (CRIEPI). Also, this study utilized the dataset of FORA-WNP30, which was produced by the Japan Agency for Marine-Earth Science and Technology (JAMSTEC) and the Meteorological Research Institute of the JMA (JMA/MRI). This work is supported by MEXT KAKENHI Grants 17H02956 and 17K14398, Joint Usage/Collaborative Research Center for Multidisciplinary Disaster Prevention Study of the Disaster Prevention Research Institute (DPRI) at Kyoto University

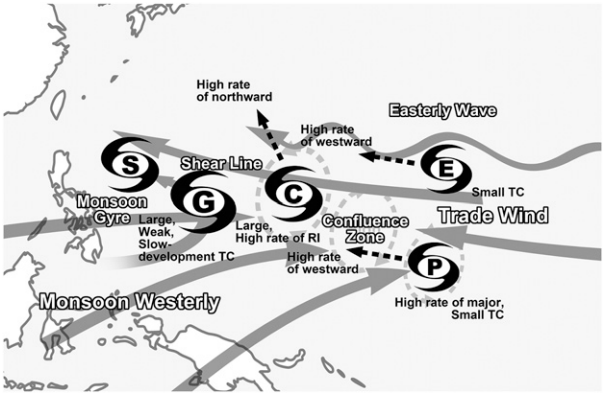

FIG. 8. Schematic image of the five flow patterns contributing to TCG based on RH99. The westerly and easterly winds are indicated by arrows, and the TCG location (cyclone symbol) of each pattern is shown.

(29G-05), Collaborative Research Project on Computer Science with High-Performance Computing at Nagoya University (2017), and the Fujitsu PRIMEHPC FX10 System (Oakleaf-FX) in the Information Technology Center of the University of Tokyo (2015, 2016).

REFERENCES

Bister, M., and K. A. Emanuel, 1998: Dissipative heating and hurricane intensity. *Meteor. Atmos. Phys.*, **65**, 233–240, https://doi.org/10.1007/BF01030791.

Camargo, S. J., K. A. Emanuel, and A. H. Sobel, 2007: Use of a genesis potential index to diagnose ENSO effects on tropical cyclone genesis. *J. Climate*, **20**, 4819–4834, https://doi.org/10.1175/JCLI4282.1.

Chen, S. S., R. A. Houze Jr., and B. E. Mapes, 1996: Multiscale variability of deep convection in relation to large-scale circulation in TOGA COARE. *J. Atmos. Sci.*, **53**, 1380–1409, https://doi.org/10.1175/1520-0469(1996)053<1380:MVODCI>2.0.CO;2.

Chu, J. H., C. R. Sampson, A. S. Levine, and E. Fukada, 2002: The Joint Typhoon Warning Center tropical cyclone best-tracks, 1945–2000. Joint Typhoon Warning Center Rep. NRL/MR/7540-02-16, 22 pp., http://www.usno.navy.mil/NOOC/nmfc-ph/RSS/jtwc/best_tracks/TC_bt_report.html.

Davis, C. A., and L. F. Bosart, 2003: Baroclinically induced tropical cyclogenesis. *Mon. Wea. Rev.*, **131**, 2730–2747, https://doi.org/10.1175/1520-0493(2003)131<2730:BITC>2.0.CO;2.

——, and ——, 2004: The TT problem: Forecasting the tropical transition of cyclones. *Bull. Amer. Meteor. Soc.*, **85**, 1657–1662, https://doi.org/10.1175/BAMS-85-11-1657.

——, and ——, 2006: The formation of Hurricane Humberto (2001): The importance of extra-tropical precursors. *Quart. J. Roy. Meteor. Soc.*, **132**, 2055–2085, https://doi.org/10.1256/qj.05.42.

Emanuel, K., 1986: An air–sea interaction theory for tropical cyclones. Part I: Steady-state maintenance. *J. Atmos. Sci.*, **43**, 585–605, https://doi.org/10.1175/1520-0469(1986)043<0585:AASITF>2.0.CO;2.

——, and D. S. Nolan, 2004: Tropical cyclone activity and global climate. *26th Conf. on Hurricanes and Tropical Meteorology*, Miami, FL, Amer. Meteor. Soc., 10A.2, https://ams.confex.com/ams/26HURR/techprogram/paper_75463.htm.

Fudeyasu, H., S. Hirose, H. Yoshioka, R. Kumazawa, and S. Yamasaki, 2014: A global view of the landfall characteristics of tropical cyclones. *Trop. Cyclone Res. Rev.*, **3**, 178–192, https://doi.org/10.6057/2014TCRR03.04.

Gray, W. M., 1968: Global view of the origin of tropical disturbances and storms. *Mon. Wea. Rev.*, **96**, 669–700, https://doi.org/10.1175/1520-0493(1968)096<0669:GVOTOO>2.0.CO;2.

——, 1998: The formation of tropical cyclones. *Meteor. Atmos. Phys.*, **67**, 37–69, https://doi.org/10.1007/BF01277501.

Heta, Y., 1990: An analysis of tropical wind fields in relation to typhoon formation over the western Pacific. *J. Meteor. Soc. Japan*, **68**, 65–77, https://doi.org/10.2151/jmsj1965.68.1_65.

——, 1991: The origin of tropical disturbances in the equatorial Pacific. *J. Meteor. Soc. Japan*, **69**, 337–351, https://doi.org/10.2151/jmsj1965.69.3_337.

Knapp, K. R., M. C. Kruk, D. H. Levinson, H. J. Diamond, and C. J. Neumann, 2010: The International Best Track Archive for Climate Stewardship (IBTrACS): Unifying tropical cyclone data. *Bull. Amer. Meteor. Soc.*, **91**, 363–376, https://doi.org/10.1175/2009BAMS2755.1.

Korty, R., S. J. Camargo, and J. Galewsky, 2012: Tropical cyclone genesis factors in simulations of the Last Glacial Maximum. *J. Climate*, **25**, 4348–4365, https://doi.org/10.1175/JCLI-D-11-00517.1.

Lander, M. A., 1994: Description of a monsoon gyre and its effects on the tropical cyclones in the western North Pacific during August 1991. *Wea. Forecasting*, **9**, 640–654, https://doi.org/10.1175/1520-0434(1994)009<0640:DOAMGA>2.0.CO;2.

Leipper, D., and D. Volgenau, 1972: Hurricane heat potential of the Gulf of Mexico. *J. Phys. Oceanogr.*, **2**, 218–224, https://doi.org/10.1175/1520-0485(1972)002<0218:HHPOTG>2.0.CO;2.

Li, T., and B. Fu, 2006: Tropical cyclogenesis associated with Rossby wave energy dispersion of a preexisting typhoon. Part I: Satellite data analyses. *J. Atmos. Sci.*, **63**, 1377–1389, https://doi.org/10.1175/JAS3692.1.

——, X. Ge, B. Wang, and Y. Zhu, 2006: Tropical cyclogenesis associated with Rossby wave energy dispersion of a preexisting typhoon. Part II: Numerical simulations. *J. Atmos. Sci.*, **63**, 1390–1409, https://doi.org/10.1175/JAS3693.1.

McDonald, N. R., 1998: The decay of cyclonic eddies by Rossby wave radiation. *J. Fluid Mech.*, **361**, 237–252, https://doi.org/10.1017/S0022112098008696.

McGauley, M. G., and D. S. Nolan, 2011: Measuring environmental favorability for tropical cyclogenesis by statistical analysis of threshold parameters. *J. Climate*, **24**, 5968–5997, https://doi.org/10.1175/2011JCLI4176.1.

Onogi, K., and Coauthors, 2007: The JRA-25 Reanalysis. *J. Meteor. Soc. Japan*, **85**, 369–432, https://doi.org/10.2151/jmsj.85.369.

Ritchie, E. A., and G. J. Holland, 1999: Large-scale patterns associated with tropical cyclogenesis in the western Pacific. *Mon. Wea. Rev.*, **127**, 2027–2043, https://doi.org/10.1175/1520-0493(1999)127<2027:LSPAWT>2.0.CO;2.

Simpson, R. H., 1974: The hurricane disaster–potential scale. *Weatherwise*, **27**, 169–186, https://doi.org/10.1080/00431672.1974.9931702.

Usui, T. Y., and Coauthors, 2017: Four-dimensional variational ocean reanalysis: A 30-year high-resolution dataset in the western North Pacific (FORA-WNP30). *J. Oceanogr.*, **73**, 205–233, https://doi.org/10.1007/s10872-016-0398-5.

Wada, A., 2015: Verification of tropical cyclone heat potential for tropical cyclone intensity forecasting in the western North Pacific. *J. Oceanogr.*, **71**, 373–387, https://doi.org/10.1007/s10872-015-0298-0.

Wang, Y., 2009: How do outer spiral rainbands affect tropical cyclone structure and intensity? *J. Atmos. Sci.*, **66**, 1250–1273, https://doi.org/10.1175/2008JAS2737.1.

Xu, J., and Y. Wang, 2010: Sensitivity of the simulated tropical cyclone inner-core size to the initial vortex size. *Mon. Wea. Rev.*, **138**, 4135–4157, https://doi.org/10.1175/2010MWR3335.1.

Yoshida, R., and H. Ishikawa, 2013: Environmental factors contributing to tropical cyclone genesis over the western North Pacific. *Mon. Wea. Rev.*, **141**, 451–467, https://doi.org/10.1175/MWR-D-11-00309.1.